MOVING-WATER EQUILIBRIA PRESERVING NONSTAGGERED CENTRAL SCHEME FOR OPEN CHANNEL FLOWS

ZHEN LI [†, ‡], JIAN DONG[§], YIMING LUO[†, ‡], MIN LIU[†, ‡], AND *DINGFANG LI[†, ‡]

Abstract. In this paper, we investigate a well-balanced and positive-preserving non-staggered central scheme, which has second-order accuracy on both time and spatial scales, for open channel flows with variable channel width and non-flat bottom. We perform piecewise linear reconstructions of the conserved variables and energy as well as discretize the source term using the property that the energy remains constant, so that the complex source term and the flux can be precisely balanced so as to maintain the steady state. The scheme also ensures that the cross-sectional wet area is positive by introducing a draining time-step technique. Numerical experiments demonstrate that the scheme is capable of accurately maintaining both the still steady-state solutions and the moving steady-state solutions, simultaneously. Moreover, the scheme has the ability to accurately capture small perturbations in the moving steady-state solution and avoid generating spurious oscillations. It is also capable of showing that the scheme is positive-preserving and robust in solving the dam-break problem.

Key words. Open-channel flows, non-staggered central schemes, second-order accuracy, moving-water steady states, well-balanced, positivity-preserving.

1. Introduction.

The widely applied shallow water equation, also called the Saint-Venant system, is usually employed to model the flow of water with a free surface under the influence of a gravitational field. It is derived from the classical Navier-stokes equation when making hydrostatic pressure assumptions and integrating over the direction of water depth. However, the classical Saint-Venant system does not take into account the variation of channel width, i.e., the variation of channel width with spatial location. But the variable channel width is of great practical importance for studying the problem of the shallow water flows through a channel, for example, to simulate the flow of water in canals and coastal areas. Therefore, it is particularly important to study the shallow water equations in channels based on the variable channel width and the non-flat bottom. The one-dimension shallow water in channels expressed in the following form:

$$\begin{cases} A_t + Q_x = 0, \\ Q_t + (\frac{Q^2}{A} + g\frac{A^2}{2\sigma})_x = g\frac{A^2}{2\sigma^2}\sigma_x - gAB_x, \end{cases} \tag{1.1}$$

where $A(x,t) := \sigma(x)h(x,t)$ denotes the wet cross-sectional area, $\sigma(x)$ denotes the channel width, $B(x)$ denotes the bottom topography, $h(x,t)$ denotes the water depth, $Q(x,t) := A(x,t)u(x,t)$ represents the discharge, $u(x,t)$ denotes the velocity. It is useful to define the water surface elevation denoted by $w(x,t) := h(x,t) + B(x)$ in constructing well-balanced schemes.

In the practical calculation of the equation (1.1), its analytical solutions tend to be nonexistent. Therefore, the investigation of steady-state solutions to the equation is a direction commonly pursued in computational fluid dynamics. For the shallow water equation, two types of steady-state solutions are usually considered, one is the still-water steady-state solution and the other is the moving-water steady-state solution. The former is a special case of the latter when the velocity is zero. The latter is more difficult to construct than the former due to the presence of nonlinear terms.

A number of solutions associated with physical phenomena are small perturbations with steady state. Accurately catching these solutions is a significant and challenging task, because the direct application of

*Corresponding author.
[†]School of Mathematics and Statistics, Wuhan University, Wuhan, Hubei, 430072, China
[‡]Hubei Key Laboratory of Computational Science, Wuhan University, Wuhan, Hubei, 430072, China
[§]Department of Mathematics, College of Liberal Arts and Science, National University of Defense Technology, Changsha, Hunan, 410073, China

shock capture methods may generate spurious oscillations. These non-physical spurious oscillations extraordinarily interfere with the simulation of physical waves. These issues can be alleviated by refining the computational meshes, however, which are expensive and impractical. Consequently, it is essential to formulate a *well-balanced* scheme to guarantee that the flux and the discretized source terms can be accurately balanced with each other when considering both the steady-state solutions. The computational error of the steady-state solution can be bounded within the machine accuracy.

To maintain the still-water steady-state solution of the open channel flow, many scholars have made great efforts to design well-balanced and positive-preserving schemes. In 1999, Vázquez-Cendón [25] proposed a well-balanced numerical scheme for shallow water equations with irregular channels but whose local cross sections are rectangular. Subsequently, Hernández-Dueñas and Karni [26] extended the cross section to shallow water equations with arbitrary cross sections and proposed a class of ROE-type upwind schemes. Balbas and Hernandez-Duenas [20, 21] proposed a numerical method to preserve the still-water steady-state solution at the wet and dry interfaces, Xing [30] designed a WENO scheme, Qian [24] constructed a higher-order discontinuous Galerkin method with well-balanced and positivity-preserving to solve the shallow water equations in channels with a non-flat bottom and irregular river width. Dong and Li [18] proposed a method based on the hydrostatic reconstruction of the discrete source term, which is also able to maintain the hydrostatic steady-state solution of the open channel flow and guarantee a positive wet area of the cross section when there is a dry-wet transition.

However, it is nontrivial to construct a discretization of source terms to maintain moving-water steady states for open channel flows or shallow water flows. Murillo and Navarro[1] proposed an algorithm to discretize source terms based on energy-balanced methods, which are able to accurately maintain the unsteady equilibrium. But, their scheme only achieves first-order accuracy on both spatial and temporal scales. A high-order discontinuous Galerkin (DG) method researched in [7, 8] accurately maintains the moving-water steady states and guarantee the positivity of the water depth. Liu developed a partial relaxation schemes which is on the basis of the finite volume method for open channels [2] and for Saint-Venant systems [3]. Both of the two steady-state-preserving numerical schemes avoid the complicated discretization of source terms and solving nonlinear equations. However, neither of these two schemes can keep the energy in equilibrium, which is equal to a constant. The central-upwind method was discussed in [4, 5, 6] to maintain the moving-water steady states of the Saint-Venant system. But, the new central-upwind scheme proposed in [6] cannot maintain the still-water steady-state solution.

Here, a non-staggered central scheme is presented to maintain the steady-state solutions of the system (1.1). The central scheme was first proposed by Nessyahu and Tadmor (NT scheme) in 1990 [9]. After that, Jiang et al.[10] in 1998, constructed a new, simpler and high-resolution non-staggered central scheme compared to the NT scheme. Then, the central scheme slowly extended to higher orders [11, 12, 13, 14, 15, 16]. Touma [22, 23] investigates an equilibrium non-staggered central finite volume method for shallow water equations with dry and wet interfaces. The method satisfies the still-water steady states by using the surface gradient method and preserves nonnegative water depth, but the method does not necessarily satisfy both conditions simultaneously. While Dong [17, 18, 19] used a hydrostatic reconstruction approach for the discretization of the source term to propose a non-staggered central scheme with both well-balanced and positivity-preserving, yet the scheme was discussed only for still-water steady-state solutions.

In this paper, a second-order non-staggered central scheme is presented, which can not only simultaneously maintain the moving-water steady state and still-water steady state for open channels, but also preserve the positivity of the wet cross-sectional area. There are two key components to designing the well-balanced scheme in this paper: the first key component is a piecewise linear reconstruction using conservation variables and energy, not just conservation variables only; the second key component is the special discretization of complex source terms, which is carried out depending on the difference of hydrostatic numerical fluxes and the constant energy. How to maintain the positivity of the A is crucial to ensure water mass conservation,

and in this paper we use the draining time step technique to obtain its properties. To our best knowledge, this work is the first to maintain the moving-water steady-state solutions using the non-staggered central scheme. We would like to emphasize that the currently proposed scheme can maintain both types of steady-state solutions simultaneously.

We summarize the main strengths of the proposed scheme:

• It is a non-staggered central scheme without solving the Riemann problem.

• It can maintain the both types of steady states: still-water and moving-water steady-states.

• It can guarantee that the wet cross-sectional area is non-negative by making use of a "draining" time-step.

• It has second-order accuracy on both time and space scales.

The paper as structured as follows. In Section 2, we present a non-staggered central scheme for open channels. Then, in Section 3, we demonstrate that the proposed scheme is well-balanced and positivity-preserving. In Section 4, some numerical experiments are used to demonstrate the properties proposed above. In Section 5, some concluding remarks are given.

2. The non-staggered central scheme.

The classical scheme consists of three parts: the forward step: calculate the cell average of the solution on the staggered grid; the corrector step: update the cell average of the solution calculated in the forward step; the backward step: compute the value on the non-staggered grid using the updated solution on the staggered grid. Before introducing the non-staggered central scheme, we first give a short overview of the steady-state solution for the hyperbolic system of balance laws. Furthermore, to simplify the calculations, we also make piecewise linear approximations for the channel width and the non-flat bottom.

The above system (1.1) has the following compact forms:

$$U_t + F(U)_x = S(U, B). \tag{2.1}$$

The $U = \begin{pmatrix} A \\ Q \end{pmatrix}$, the flux $F(U) = \begin{pmatrix} Q \\ \frac{Q^2}{A} + g\frac{A^2}{2\sigma} \end{pmatrix}$ and source terms $S(U,B) = \begin{pmatrix} 0 \\ g\frac{A^2}{2\sigma^2}\sigma_x - gAB_x \end{pmatrix}$, respectively. For the equation (2.1), the equilibrium between the $F(U)$ and the $S(U,B)$ corresponds to various non-trivial equilibrium solutions, namely steady-state solutions. When the flow lies in a steady regime, the system (2.1) admits

$$Q \equiv \text{Const}, \quad E := \frac{1}{2}\frac{Q^2}{A^2} + g(\frac{A}{\sigma} + B) \equiv \text{Const}, \tag{2.2}$$

in which E denotes the energy. The above solutions are known as the moving-water steady-state solutions. We mainly focus in this paper on how to construct a moving-water steady-state-preserving scheme.

Notice that when $Q \equiv 0$, we derive a physical-related steady-state solutions, i.e., the still-water steady states:

$$Q \equiv 0, \qquad \frac{A}{\sigma} + B \equiv \text{Const}. \tag{2.3}$$

2.1. Piecewise linear approximations of the channel width and the bottom topography.

For purposes of simplicity, we discretize the space domain with $x_j := j\Delta x$, where j is any spatial index that can be a half-integer or an integer, and Δx is the spatial scale. We use C_j to denote the non-staggered

cells $C_j := [x_{j-\frac{1}{2}}, x_{j+\frac{1}{2}}]$ and $C_{j+\frac{1}{2}}$ the staggered cells $C_{j+\frac{1}{2}} := [x_j, x_{j+1}]$. Suppose the cell average of the variable

$$\bar{U}_j^n \approx \frac{1}{\Delta x}\int_{x_{j-\frac{1}{2}}}^{x_{j+\frac{1}{2}}} U(x,t^n)dx, \tag{2.4}$$

is available.

As is known to all, when the channel width function is complicated, it is expensive to compute the cell average of $\sigma(x)$ exactly. Therefore, before proceeding to the first evolution step, for simplicity of computation, we use $\hat{\sigma}(x)$, which is continuous piecewise linear functions, to approximate the $\sigma(x)$.

$$\hat{\sigma}(x) = \sigma_{j-\frac{1}{2}} + (\sigma_{j+\frac{1}{2}} - \sigma_{j-\frac{1}{2}}) \cdot \frac{x - x_{j-\frac{1}{2}}}{\Delta x}, \quad x \in [x_{j-\frac{1}{2}}, x_{j+\frac{1}{2}}], \tag{2.5}$$

where

$$\sigma_{j+\frac{1}{2}} := \frac{1}{2}[\sigma(x_{j+\frac{1}{2}} + 0) + \sigma(x_{j+\frac{1}{2}} - 0)].$$

If the channel width σ is continuous at $x = x_{j+\frac{1}{2}}$, then the above equation can be simplified to $\sigma_{j+\frac{1}{2}} = \sigma(x_{j+\frac{1}{2}})$.

Notice that by the definition of the $\hat{\sigma}$ function, we have the following equation holds:

$$\sigma_j := \hat{\sigma}(x_j) = \frac{1}{\Delta x}\int_{x_{j-\frac{1}{2}}}^{x_{j+\frac{1}{2}}} \hat{\sigma}(x)dx = \frac{1}{2}(\sigma_{j-\frac{1}{2}} + \sigma_{j+\frac{1}{2}}). \tag{2.6}$$

Similarly, we use $\hat{B}(x)$, which is continuous piecewise linear functions, to approximate the $B(x)$:

$$\hat{B}(x) = B_{j-\frac{1}{2}} + (B_{j+\frac{1}{2}} - B_{j-\frac{1}{2}}) \cdot \frac{x - x_{j-\frac{1}{2}}}{\Delta x}, \quad x \in [x_{j-\frac{1}{2}}, x_{j+\frac{1}{2}}], \tag{2.7}$$

and define:

$$B_j := \hat{B}(x_j) = \frac{1}{\Delta x}\int_{x_{j-\frac{1}{2}}}^{x_{j+\frac{1}{2}}} \hat{B}(x)dx = \frac{1}{2}(B_{j-\frac{1}{2}} + B_{j+\frac{1}{2}}). \tag{2.8}$$

REMARK 2.1. *The order of the non-staggered central schemes in this paper is not altered by approximating B, σ with $\tilde{B}$ and $\tilde{\sigma}$ because the piecewise linear interpolations* (2.7) *and* (2.5) *are second-order accurate for smooth B and σ.*

2.2. The forward step.

For the well-balanced property, a major component of the scheme is the reconstruction of the variable $V = (A, Q, E)^T$ rather than conservative variable $U = (A, Q)^T$. To this end, we compute the energy:

$$E_j = \frac{\bar{Q}_j^2}{2\bar{A}_j^2} + g(\frac{\bar{A}_j}{\sigma_j} + B_j). \tag{2.9}$$

To achieve non-oscillatory characteristics and second-order accuracy in spatial dimensions, we approximate the variable $V(x,t^n)$ by using piecewise linear functions:

$$P_j(x,t^n) = \bar{V}_j^n + (x - x_j)(\bar{V}_j^n)', \quad x \in C_j, \tag{2.10}$$

where the numerical derivative $(\bar{V}_j^n)'$ is of first order, which is calculated by nonlinear limiters. For all numerical experiments in Section 4, we choose the following limiter [9].

$$(\bar{V}_j^n)' = \text{minmod}\left(\theta\frac{\bar{V}_j^n - \bar{V}_{j-1}^n}{\Delta x}, \quad \frac{\bar{V}_{j+1}^n - \bar{V}_{j-1}^n}{2\Delta x}, \quad \theta\frac{\bar{V}_{j+1}^n - \bar{V}_j^n}{\Delta x}\right), \quad \theta \in [1,2], \tag{2.11}$$

and

$$\text{minmod}(a,b,c) = \begin{cases} \max(a,b,c), & \max(a,b,c) < 0, \\ \min(a,b,c), & \min(a,b,c) > 0, \\ 0, & \text{otherwise}, \end{cases}$$

and the parameter θ is used to control the numerical dissipation. It is well known that the bigger the value of the parameter θ, the smaller the corresponding dissipation, i.e., more oscillatory reconstruction is required, see [22].

Equipped with $P_j(x,t^n)$, we can calculate the left and right point values $V^{\pm}_{j+\frac{1}{2}}$:

$$V^{-}_{j+\frac{1}{2}} = \bar{V}^n_j + \frac{\Delta x}{2}(\bar{V}^n_j)', \quad V^{+}_{j+\frac{1}{2}} = \bar{V}^n_{j+1} - \frac{\Delta x}{2}(\bar{V}^n_{j+1})', \tag{2.12}$$

and calculate the cell average:

$$\begin{aligned} \bar{V}^n_{j+\frac{1}{2}} &= \frac{1}{\Delta x}\left(\int_{x_j}^{x_{j+\frac{1}{2}}} P_j(x,t^n)dx + \int_{x_{j+\frac{1}{2}}}^{x_{j+1}} P_{j+1}(x,t^n)dx\right) \\ &= \frac{1}{2}(P_j(x_{j+\frac{1}{4}},t^n) + P_{j+1}(x_{j+\frac{3}{4}},t^n)) \\ &= \frac{1}{2}(\bar{V}^n_{j+1} + \bar{V}^n_j) - \frac{\Delta x}{8}((\bar{V}^n_{j+1})' - (\bar{V}^n_j)'). \end{aligned} \tag{2.13}$$

However, if we use the above information for the next evolution step, the energy cannot be maintained a constant. Therefore, we need to compute the corresponding values $\bar{A}_{j+\frac{1}{2}}$ by solving the cubic equation

$$\frac{\bar{Q}^2_{j+\frac{1}{2}}}{2A^2} + g(\frac{A}{\bar{\sigma}_{j+\frac{1}{2}}} + \bar{B}_{j+\frac{1}{2}}) - \bar{E}_{j+\frac{1}{2}} = 0 \tag{2.14}$$

where

$$\bar{B}_{j+\frac{1}{2}} = \frac{1}{\Delta x}\int_{x_j}^{x_{j+1}} \tilde{B}(x)dx = \frac{1}{4}(B_j + 2B_{j+\frac{1}{2}} + B_{j+1}), \tag{2.15}$$

$$\bar{\sigma}_{j+\frac{1}{2}} = \frac{1}{\Delta x}\int_{x_j}^{x_{j+1}} \tilde{\sigma}(x)dx = \frac{1}{4}(\sigma_j + 2\sigma_{j+\frac{1}{2}} + \sigma_{j+1}). \tag{2.16}$$

The procedure for solving such the cubic equations and certain criteria for determining which non-trivial root to choose will be discussed in Subsection 2.2.1. Ultimately, we obtain $\bar{V}^n_{j+\frac{1}{2}}$ in the forward step.

2.2.1. The solution of the nonlinear equation.

Here, we present the procedure for finding the solution of the cubic equation mentioned above in this section. Given σ, B, Q and E, equation (2.14) can be simplified to a nonlinear algebraic equation as shown below:

$$\varphi(A) := \frac{Q^2}{2A^2} + g(\frac{A}{\sigma} + B) - E = 0. \tag{2.17}$$

When solving the equation (2.17), the solutions obtained is probably not unique, so we are required to select physically relevant solutions. The process is as follows.

If the discharge $Q = 0$, the equation (2.17) degenerates into a linear equation $\varphi(A) := g(\frac{A}{\sigma} + B) - E = 0$ and the solution is:

$$A = (\frac{\sigma E}{g} - \sigma B).$$

If $Q \neq 0$, since $\varphi(A)$ is convex function, it reaches a minimum value at

$$A_0 = \sqrt[3]{\frac{\sigma Q^2}{g}}.$$

In fact, we call the point corresponding to A_0 the sonic point, at which the Froude number

$$Fr := \sqrt{\sigma}|u|/\sqrt{gA} = \sqrt{\sigma}|Q|/\sqrt{gA^3} = 1,$$

at $A = A_0$. When $A > A_0$ ($A < A_0$), there is $Fr < 1$ ($Fr > 1$), and its corresponding state is called subsonic (supersonic).

If $\varphi(A_0) > 0$, the equation (2.17) has no positive root, thus we still select the original reconstructed value A; if $\varphi(A_0) = 0$, the equation has only one positive root $A = A_0$; if $\varphi(A_0) < 0$, the equation has three roots:

$$A = 2\sqrt[3]{\hat{P}}\cos(\hat{T} + \frac{2k\pi}{3}) - \frac{1}{3}(\sigma B - \frac{\sigma E}{g}), \quad k = 0, 1, 2, \tag{2.18}$$

where

$$\hat{P} = \sqrt{-(\frac{P}{3})^3}, \qquad \hat{T} = \frac{1}{3}\arccos(-\frac{T}{2\hat{P}}),$$

$$P = -\frac{1}{3}(\sigma B - \frac{\sigma E}{g}), \qquad T = \frac{\sigma Q^2}{2g} + \frac{2}{27}(\sigma B - \frac{\sigma E}{g})^3.$$

It is observed that one of these three root is negative, while the other two are positive. Thus, we discard the negative root and select the physically relevant root as follows: if the states of two adjacent dual cells are supersonic, we choose the smaller of the two positive roots; if it is subsonic, we choose the larger one; otherwise, we choose the one that is closer to the reconstructed value.

2.3. The discretization of the flux and the source term in the corrector step.

For the sake of updating the variables, we integrate equation (2.1) on the rectangle $C_{j+\frac{1}{2}} \times [t^n, t^{n+1}]$:

$$\begin{aligned}\frac{1}{\Delta x}\int_{x_j}^{x_{j+1}}(U(x,t^{n+1}) - U(x,t^n))dx = &-\frac{1}{\Delta x}\int_{t^n}^{t^{n+1}}(F(U(x_{j+1},t)) - F(U(x_j,t)))dt \\ &+ \frac{1}{\Delta x}\int_{x_j}^{x_{j+1}}\int_{t^n}^{t^{n+1}} S(U,B)dtdx.\end{aligned} \tag{2.19}$$

At t^{n+1} and $x \in C_{j+\frac{1}{2}}$, we suppose that $U(x,t^{n+1}) \approx P_{j+\frac{1}{2}}(x,t^{n+1})$ is a piecewise linear function. The Mean-Value theorem gives:

$$\frac{1}{\Delta x}\int_{x_j}^{x_{j+1}} U(x,t^{n+1})dx \approx \bar{U}_{j+\frac{1}{2}}^{n+1}, \tag{2.20}$$

which makes the first half of equation (2.19) become

$$\frac{1}{\Delta x}\int_{x_j}^{x_{j+1}}(U(x,t^{n+1}) - U(x,t^n))dx \approx \bar{U}_{j+\frac{1}{2}}^{n+1} - \bar{U}_{j+\frac{1}{2}}^{n}.$$

We now concentrate on the second half of equation (2.19), which is essential for maintaining the well-balanced property. On the other hand, to ensure that the scheme has second-order accuracy on the time scale, we adopt the midpoint product rules to the fluxes:

$$\frac{1}{\Delta t}\int_{t^n}^{t^{n+1}} F(U(x_j,t))dt \approx F(\bar{U}_j^{n+\frac{1}{2}}), \tag{2.21}$$

where $\bar{U}_j^{n+\frac{1}{2}}$ is available through a first-order Taylor expansion:

$$\bar{U}_j^{n+\frac{1}{2}} := \bar{U}_j^n + \frac{\Delta t}{2}(-(F_j^n)' + S_j^n), \tag{2.22}$$

with $(F_j^n)'$ approximates the flux divergence and S_j^n approximates the source term. Depending on the specific forms of $F(U)_x$ and $S(U,B)$, $(F_j^n)'$ and S_j^n can be defined as follows:

$$(F_j^{'}) := \begin{pmatrix} (Q_j)' \\ A_j(E_j^{'} - gB_j^{'}) + u_j(Q_j)' + \frac{g}{2}(\frac{A_j}{\sigma_j})^2(\sigma_j)' \end{pmatrix}, \quad S_j := \begin{pmatrix} 0 \\ \frac{g}{2}(\frac{A_j}{\sigma_j})^2(\sigma_j)' - gA_j(B_j)' \end{pmatrix},$$

with

$$(B_j)' = \frac{B_{j+\frac{1}{2}} - B_{j-\frac{1}{2}}}{\Delta x}, \quad (\sigma_j)' = \frac{\sigma_{j+\frac{1}{2}} - \sigma_{j-\frac{1}{2}}}{\Delta x}.$$

On the other hand, for integrations of source terms in equation (2.19), the midpoint quadrature rule is used to approximate it:

$$\int_{x_j}^{x_{j+1}}\int_{t^n}^{t^{n+1}} S(U)dtdx \approx \Delta x \Delta t S(\bar{U}_j^{n+\frac{1}{2}}, \bar{U}_{j+1}^{n+\frac{1}{2}}), \tag{2.23}$$

with

$$S(\bar{U}_j, \bar{U}_{j+1}) = \begin{pmatrix} 0 \\ -g \cdot \frac{A_{j+1}+A_j}{2} \cdot \frac{B_{j+1}-B_j}{\Delta x} + \frac{g}{2} \cdot \frac{A_j}{\sigma_j} \cdot \frac{A_{j+1}}{\sigma_{j+1}} \cdot \frac{\sigma_{j+1}-\sigma_j}{\Delta x} + \frac{A_{j+1}-A_j}{4\Delta x} \cdot (u_j - u_{j+1})^2 \end{pmatrix}. \tag{2.24}$$

since the term $(u_j - u_{j+1})^2 = O((\Delta x)^2)$ for smooth solutions, the equation (2.24) is second-order accuracy.

Remark 2.2. *The derivation of quadrature* (2.24) *can refer to Theorem 3.1 in Section 3, which takes advantage of the characteristic of constant energy.*

Combining with equations (2.21) and (2.23), equation (2.19) is simplified to

$$\bar{U}_{j+\frac{1}{2}}^{n+1} = \bar{U}_{j+\frac{1}{2}}^n - \frac{\Delta t}{\Delta x}(F(\bar{U}_{j+1}^{n+\frac{1}{2}}) - F(\bar{U}_j^{n+\frac{1}{2}})) + \Delta t S(\bar{U}_j^{n+\frac{1}{2}}, \bar{U}_{j+1}^{n+\frac{1}{2}}). \tag{2.25}$$

From equation (2.25), it is clear that the variable $\bar{U}_{j+\frac{1}{2}}^{n+1} = (\bar{A}_{j+\frac{1}{2}}^{n+1}, \bar{Q}_{j+\frac{1}{2}}^{n+1})^T$ is obtained. Once again, the energy $\bar{E}_{j+\frac{1}{2}}^{n+1}$ is computed as follows:

$$\bar{E}_{j+\frac{1}{2}} = \frac{1}{2}\frac{\bar{Q}_{j+\frac{1}{2}}^2}{\bar{A}_{j+\frac{1}{2}}^2} + g(\frac{\bar{A}_{j+\frac{1}{2}}}{\bar{\sigma}_{j+\frac{1}{2}}} + \bar{B}_{j+\frac{1}{2}}). \tag{2.26}$$

Hence, we ultimately update the variable $\bar{V}_{j+\frac{1}{2}}^{n+1}$ in the corrector step.

REMARK 2.3. *We observe that, in the (almost) dry region, the calculated value of A may be greatly small. It may lead to the computed value of the u artificially large. Therefore, we desingularize the calculation of the u:*

$$u = \begin{cases} \frac{Q}{A}, A > \epsilon, \\ 0, \text{ otherwise}, \end{cases} \tag{2.27}$$

where ϵ is taken 10^{-12} in all numerical experiments of this paper. However, for consistency, the discharge is recomputed using $Q = A \cdot u$.

2.4. The backward step.

To resume the variable on cell $C_{j+\frac{1}{2}}$, we use the following piecewise linear function.

$$P_{j+\frac{1}{2}}(x, t^{n+1}) = \bar{V}^{n+1}_{j+\frac{1}{2}} + (x - x_{j+\frac{1}{2}})(\bar{V}^{n+1}_{j+\frac{1}{2}})',$$

which is based on the values (2.25) and (2.26). The minmod limiter is chosen to satisfy the properties of non-oscillatory. Then, the cell average of V is computed as

$$\bar{V}^{n+1}_j = \frac{1}{2}(\bar{V}^{n+1}_{j-\frac{1}{2}} + \bar{V}^{n+1}_{j+\frac{1}{2}}) - \frac{\Delta x}{8}((\bar{V}^{n+1}_{j+\frac{1}{2}})' - (\bar{V}^{n+1}_{j-\frac{1}{2}})'). \tag{2.28}$$

Likewise, to maintain the steady states, we solve the following nonlinear equation to replace the reconstructed variable $\bar{A}^{n+1}_j$ based on the $\bar{Q}^{n+1}_j$ and $\bar{E}^{n+1}_j$:

$$\frac{\bar{Q}^2_j}{2A^2} + g(\frac{A}{\sigma_j} + B_j) - \bar{E}_j = 0. \tag{2.29}$$

According to Subsection 2.2.1, we select the physically relevant solution of equation (2.29). So far we get the variable V^{n+1}_j at t^{n+1} on the non-staggered cells.

3. Theoretical analysis of the scheme.

Here, we certify that the scheme maintains the steady states (2.2) and (2.3) at the discrete levels. That is, the proposed scheme is well balanced to accurately capture small perturbations and avoid generating spurious oscillations. Meanwhile, we utilize a "draining" time-step to prove the positivity-preserving property, which maintains the water mass conservation.

3.1. The well-balancing property.

Here, we demonstrate that the scheme can preserve both moving-water steady-state solutions and still-water steady-state solutions by means of two theorems. First see Theorem 3.1, that the currently proposed scheme has well-balanced property for moving water.

THEOREM 3.1. *The numerical solution $\bar{U}^n_j$ assumes that, at time level t^n, satisfies the constraints* (2.2)*, i.e.,*

$$Q_j \equiv \hat{Q} \quad \textit{and} \quad E_j \equiv \hat{E}, \quad \forall j \in \mathbb{Z}. \tag{3.1}$$

Then,

(*a*) *the solution obtained from equation* (2.22) *is $\bar{U}^{n+\frac{1}{2}}_j = \bar{U}^n_j$;*

(*b*) *the solution obtained from equation* (2.25) *and the solution obtained from equation* (2.14) *are equal, i.e., $\bar{U}^{n+1}_{j+\frac{1}{2}} = \bar{U}^n_{j+\frac{1}{2}}$;*

(*c*) *utilizing the forward projection and backward projection, the currently proposed scheme is well-balanced, that is,* $\bar{U}_j^{n+1} = \bar{U}_j^n$.

Proof. Firstly, we proof (*a*). According to the condition (3.1), it has

$$(Q_j)' = 0 \quad and \quad (E_j)' = 0, \quad \forall j \in \mathbb{Z}.$$

Therefore, $(F_j)'$ and S_j have the following forms:

$$(F_j') = \begin{pmatrix} 0 \\ -gA_j(B_j)' + \frac{g}{2}(\frac{A_j}{\sigma_j})^2(\sigma_j)' \end{pmatrix}, \quad S_j = \begin{pmatrix} 0 \\ \frac{g}{2}(\frac{A_j}{\sigma_j})^2(\sigma_j)' - gA_j(B_j)' \end{pmatrix}.$$

Then, the prediction step (2.22) becomes

$$\begin{aligned} \bar{U}_j^{n+\frac{1}{2}} &= \bar{U}_j^n + \frac{\Delta t}{2}\left[-\begin{pmatrix} 0 \\ -gA_j(B_j)' + \frac{g}{2}(\frac{A_j}{\sigma_j})^2(\sigma_j)' \end{pmatrix} + \begin{pmatrix} 0 \\ \frac{g}{2}(\frac{A_j}{\sigma_j})^2(\sigma_j)' - gA_j(B_j)' \end{pmatrix} \right] \\ &= \bar{U}_j^n. \end{aligned}$$

Next, we proof (*b*), which shows $U_{j+\frac{1}{2}}^{n+1} = U_{j+\frac{1}{2}}^n$. With consideration of part (*a*) of Theorem 3.1, the time evolution step (2.25) becomes

$$\bar{U}_{j+\frac{1}{2}}^{n+1} = \bar{U}_{j+\frac{1}{2}}^n - \frac{\Delta t}{\Delta x}(F(\bar{U}_{j+1}^n) - F(\bar{U}_j^n)) + \Delta t S(\bar{U}_{j+1}^n, \bar{U}_j^n), \tag{3.2}$$

where the flux is

$$\begin{aligned} F^{(2)}(\bar{U}_{j+1}) - F^{(2)}(\bar{U}_j) &= \hat{Q}^2(\frac{1}{A_{j+1}} - \frac{1}{A_j}) + \frac{g}{2}(\sigma_{j+1}h_{j+1}^2 - \sigma_j h_j^2) \\ &= \hat{Q}^2(\frac{1}{A_{j+1}} - \frac{1}{A_j}) + \frac{g}{2}(\sigma_{j+1}h_{j+1} + \sigma_j h_j)(h_{j+1} - h_j) + h_{j+1}h_j(\sigma_{j+1} - \sigma_j). \end{aligned} \tag{3.3}$$

Since the $E_{j+1} = E_j$, it has

$$gh_{j+1} - gh_j = \frac{\hat{Q}^2}{2}(\frac{1}{A_j^2} - \frac{1}{A_{j+1}^2}) + gB_j - gB_{j+1}. \tag{3.4}$$

The flux in equation (3.2) is finally simplified as:

$$F(\bar{U}_{j+1}) - F(\bar{U}_j) = \begin{pmatrix} 0 \\ g\frac{A_{j+1}+A_j}{2}(B_j - B_{j+1}) + g\frac{h_j h_{j+1}}{2}(\sigma_{j+1} - \sigma_j) + \frac{A_{j+1}-A_j}{4}(\frac{\hat{Q}}{A_{j+1}} - \frac{\hat{Q}}{A_j})^2 \end{pmatrix}.$$

Then, considering the source term (2.24), the two parts of equation (3.2) are

$$-\frac{\Delta t}{\Delta x}(F(\bar{U}_{j+1}^n) - F(\bar{U}_j^n)) + \Delta t S(\bar{U}_j^n, \bar{U}_{j+1}^n) = \begin{pmatrix} 0 \\ 0 \end{pmatrix},$$

so it has $\bar{U}_{j+\frac{1}{2}}^{n+1} = \bar{U}_{j+\frac{1}{2}}^n$.

Finally, we proof (*c*). Suppose that the states of C_{j-1}, C_j, and C_{j+1} are supersonic, i.e., $Fr > 1$. In the forward projection,

$$Q_{j-\frac{1}{2}}^n = Q_{j+\frac{1}{2}}^n = \hat{Q}, \quad E_{j-\frac{1}{2}}^n = E_{j+\frac{1}{2}}^n = \hat{E}.$$

Since the minmod parameter $\theta \in [1,2]$, the reconstructed value of A satisfies

$$A^n_{j\pm\frac{1}{2}} \in [\min(A^n_{j+1}, A^n_j, A^n_{j-1}),\ \max(A^n_{j+1}, A^n_j, A^n_{j-1})].$$

By the process of solving the nonlinear equations and selecting the physically relevant solutions method in subsection 2.2.1, we obtain that the states of $C_{j-\frac{1}{2}}$ and $C_{j+\frac{1}{2}}$ are supersonic, that is, $Fr > 1$. According to Parts (a) and (b) of Theorem 3.1, the time evolution will not change the conservative variables and energy. Similarly, in the backward projection,

$$Q^{n+1}_j = \hat{Q}, \quad E^{n+1}_j = \hat{E},$$

the state of C_j is supersonic, which leads to

$$A^{n+1}_j = A^n_j.$$

The subsonic state can also be demonstrated by a similar operation. Therefore, it can be derived that if steady states are achieved at t^n, then it will also remain unchanged at t^{n+1}. □

Then, it is shown that the currently proposed scheme can accurately maintain the steady states (2.3).

THEOREM 3.2. *The solution $\bar{U}^n_j$ assumes that, at time level t^n, satisfies the still-water steady-state constraints* (2.3)*, i.e.,*

$$Q_j \equiv 0 \quad \textit{and} \quad \frac{A_j}{\sigma_j} + B_j = \text{Const.} \tag{3.5}$$

Then, $U^{n+1}_j = U^n_j$.

Proof. For the conservative law (2.1), since $Q_j \equiv 0$, the source term (2.24) is simplified to the following form:

$$S^{(2)}_{j+\frac{1}{2}} = -g\frac{A_{j+1}+A_j}{2}\cdot\frac{B_{j+1}-B_j}{\Delta x} + \frac{g}{2}\frac{A_{j+1}}{\sigma_{j+1}}\cdot\frac{A_j}{\sigma_j}\cdot\frac{\sigma_{j+1}-\sigma_j}{\Delta x}. \tag{3.6}$$

Since the still-water steady states satisfy $\frac{A_j}{\sigma_j} + B_j = \text{Const}$, we can obtain

$$B_{j+1} - B_j = \frac{A_j}{\sigma_j} - \frac{A_{j+1}}{\sigma_{j+1}}. \tag{3.7}$$

Using the proposed discretization (3.6) and the relation (3.7), source term can be simplified:

$$\begin{aligned} S^{(2)}_{j+\frac{1}{2}} &= -\frac{g}{2}\frac{A_{j+1}+A_j}{\Delta x}\cdot\left(\frac{A_j}{\sigma_j} - \frac{A_{j+1}}{\sigma_{j+1}}\right) + \frac{g}{2}\frac{A_{j+1}}{\sigma_{j+1}}\cdot\frac{A_j}{\sigma_j}\cdot\frac{\sigma_{j+1}-\sigma_j}{\Delta x} \\ &= \frac{g}{2\Delta x}\cdot\left(\frac{A^2_{j+1}}{\sigma_{j+1}} - \frac{A^2_j}{\sigma_j}\right). \end{aligned}$$

As for the flux (3.3) is simplified to

$$F^{(2)}_{j+1} - F^{(2)}_j = \frac{g}{2}\left(\frac{A^2_{j+1}}{\sigma_{j+1}} - \frac{A^2_j}{\sigma_j}\right).$$

With part (a) in Theorem 3.1, equation (3.2) are

$$-\frac{\Delta t}{\Delta x}(F^{(2)}(\bar{U}^n_{j+1}) - F^{(2)}(\bar{U}^n_j)) + \Delta t S^{(2)}(\bar{U}^n_j, \bar{U}^n_{j+1}) = 0,$$

which demonstrates that $U^{n+1}_j = U^n_j$. □

3.2. The positivity-preserving property.

Here, we demonstrate that the currently proposed scheme has positivity-preserving property. In order to ensure A positivity, we introduce a "draining" time-step to eliminate this problem.

THEOREM 3.3. *Suppose that at time level t^n, for $j \in \mathbb{Z}$, the values of h_j, h_{j+1}, $h^+_{j+\frac{1}{2}}$, and $h^-_{j+\frac{1}{2}}$ are all non-negative. If the CFL satisfies:*

$$\begin{aligned} \lambda a \le 1, \lambda = \frac{\Delta t}{\Delta x}, \\ a = \max_j(|u_j| + \sqrt{gh_j},\ |u^-_{j+\frac{1}{2}}| + \sqrt{gh^-_{j+\frac{1}{2}}},\ |u_{j+\frac{1}{2}}| + \sqrt{gh_{j+\frac{1}{2}}},\ |u^+_{j+\frac{1}{2}}| + \sqrt{gh^+_{j+\frac{1}{2}}}), \end{aligned} \tag{3.8}$$

then, we obtain $A^{n+\frac{1}{2}}_j \ge 0$, for all $j \in \mathbb{Z}$.

Proof. With Remark 2.3, the first component of equation (2.22) can be written as:

$$\begin{aligned} \bar{A}^{n+\frac{1}{2}}_j &= \bar{A}^n_j - \frac{\Delta t}{2} \cdot (\bar{Q}^n_j)' \\ &= \bar{A}^n_j + \lambda \cdot (\frac{Q^-_{j+\frac{1}{2}} + Q^+_{j-\frac{1}{2}}}{2} - Q^-_{j+\frac{1}{2}}) \\ &= \frac{1}{2}(A^-_{j+\frac{1}{2}} + A^+_{j-\frac{1}{2}}) + \frac{\lambda}{2}(A^-_{j+\frac{1}{2}}u^-_{j+\frac{1}{2}} + A^+_{j-\frac{1}{2}}u^+_{j-\frac{1}{2}}) - \lambda A^-_{j+\frac{1}{2}}u^-_{j+\frac{1}{2}} \\ &= (\frac{1}{2} - \frac{\lambda}{2}u^-_{j+\frac{1}{2}}) \cdot A^-_{j+\frac{1}{2}} + (\frac{1}{2} + \frac{\lambda}{2}u^+_{j-\frac{1}{2}}) \cdot A^+_{j-\frac{1}{2}}, \end{aligned}$$

According to the CFL conditions: $\lambda a \le 1$ and (3.8), all coefficients are non-negative, then $\bar{A}^{n+\frac{1}{2}}_j \ge 0$. ∎

To ensure the positivity of $\bar{A}^{n+1}_{j+\frac{1}{2}}$, we insert the "draining" time step (see [25]):

$$\Delta t^{(\text{drain})}_{j+\frac{1}{2}} := \frac{\Delta x \bar{A}^n_{j+\frac{1}{2}}}{\max(0, F^{(1)}_{j+1}) + \max(0, -F^{(1)}_j)},$$

where the F is computed at time level $t = t^{n+\frac{1}{2}}$. The "draining" time step is defined as the time at which the water included in cell j leaves through the outflow flux at the beginning of the time step. Then, the evolution of A is replaced with

$$\bar{A}^{n+1}_{j+\frac{1}{2}} = \bar{A}^n_{j+\frac{1}{2}} - \frac{\Delta t^{(\text{drain})}_{j+1} F^{(1)}_{j+1} - \Delta t^{(\text{drain})}_j F^{(1)}_j}{\Delta x},$$

where

$$\Delta t^{(\text{drain})}_j = \min(\Delta t, \Delta t^{(\text{drain})}_i), \quad i = j - \frac{1}{2}\text{sgn}(F^{(1)}_j).$$

So, we have $\bar{A}^{n+1}_{j+\frac{1}{2}} \ge 0$.

REMARK 3.4. *If the two-dimension case of open channel flow is considered, since the flow is divergence-free and not just constant, this is a more difficult task and is out of the scope of this manuscript.*

4. Numerical experiments.

Here, we use some classical numerical experiments from other papers to verify the performance of the proposed scheme (the New scheme) for maintaining the steady states. In addition, we also compare it with the scheme (the Old scheme) in the literature [18] that maintains still-water steady states as a way to illustrate the advantages of currently proposed schemes. Among experiments conducted below, we have common parameters where the gravitational acceleration $g = 9.812$, the minmod parameter $\theta = 1.3$ and the computation domain and the CFL condition number $CFL = 0.35$. The computational domain of all numerical experiments is $[0, 25]$, except for the first experiment which is $[0, 1]$.

Table 4.1 L^1-errors and convergence rates.

Number of grid cells	A		Q	
	L^1-error	Rate	L^1-error	Rate
100	1.01e-02	-	7.34e-02	-
200	3.10e-03	1.70	2.07e-02	1.83
400	8.29e-04	1.90	5.52e-03	1.90
800	2.06e-04	2.00	1.40e-03	1.98
1600	5.11e-05	2.01	3.48e-04	2.00

4.1. Accuracy Test.

In this experiment we will verify whether the scheme proposed in this paper has second-order accuracy on the spatial scale. The experiment is taken from reference [28]. However, what is a bit different from reference [28] is the addition of an irregular channel width function. The bottom topography and the channel width are:

$$B(x) = [\sin(\pi x)]^2, \quad \sigma(x) = 0.9 + 0.4 \cdot (x - 0.5)^2,$$

other data are

$$A(x, 0) = \sigma(x) \cdot [5 + e^{\cos(2\pi x)}], \quad Q(x, 0) = \sigma(x) \cdot \sin(\cos(2\pi x)).$$

The experiment is done using periodic boundary conditions. The exact solution for this experimental case is not directly computable for us. Therefore, we try to use the reference solution calculated when the grid N is taken as 8000 as the exact solution to facilitate the calculation of the numerical error. We set the experiment to end at $t = 0.1$, when the shock is not yet formed and the solution is smooth. In Table 4.1, we measure the L^1-errors as well as the convergence rates corresponding to the conservative variables A and Q, respectively, at different grid sizes. The scheme proposed in this paper is easy to read from the Table 4.1 with second-order accuracy on the spatial scale.

4.2. Steady-state solution of still-water.

In this experiment we wish to verify whether the scheme proposed in this paper has the well-balanced property of convergence to the still-water steady states. And, we also compared it with the method proposed in the reference [18]. The bottom topography and channel width are:

$$B(x) = \begin{cases} 0.2 - 0.05(x - 10)^2, & 8 \le x \le 12, \\ 0.48 - 0.03(x - 17)^2, & 13 \le x \le 21, \\ 0, & \text{otherwise}, \end{cases}$$

$$\sigma(x) = \begin{cases} 0.28 + 0.005(x - 13)^2, & 5 \le x \le 21, \\ 0.6, & \text{otherwise}, \end{cases}$$

other data are

$$A(x, 0) = \sigma(x) \cdot [0.6 - B(x)], \qquad Q(x, 0) \equiv 0.$$

We use the transmissive boundary conditions and set the experiment to end at $t = 20$.

Table 4.2 L^1-errors of these two schemes at $t = 20$ at still-water steady states.

Number of grid cells	A		Q		E	
	New	Old	New	Old	New	Old
50	2.4425e-15	2.6645e-15	2.3705e-14	9.3106e-15	3.2863e-14	2.9754e-14
250	1.1580e-14	3.5194e-15	3.1767e-14	1.8910e-14	1.0818e-13	3.8902e-14
1000	2.6731e-14	1.8649e-14	9.9132e-14	5.2291e-14	2.6594e-13	1.8203e-13

On the one hand, Figure 4.1 demonstrates the results at $t = 20$. We can notice that both the schemes can exactly maintain the still-water steady states. On the other hand, we compute L^1-errors for these two schemes and show the obtained results in Tables 4.2. It is indeed clear to us that their L^1-errors are in the same order of magnitude, i.e., the machine precision. Even with a relatively coarse grid, both schemes has the well-balanced property of convergence to the still-water steady states.

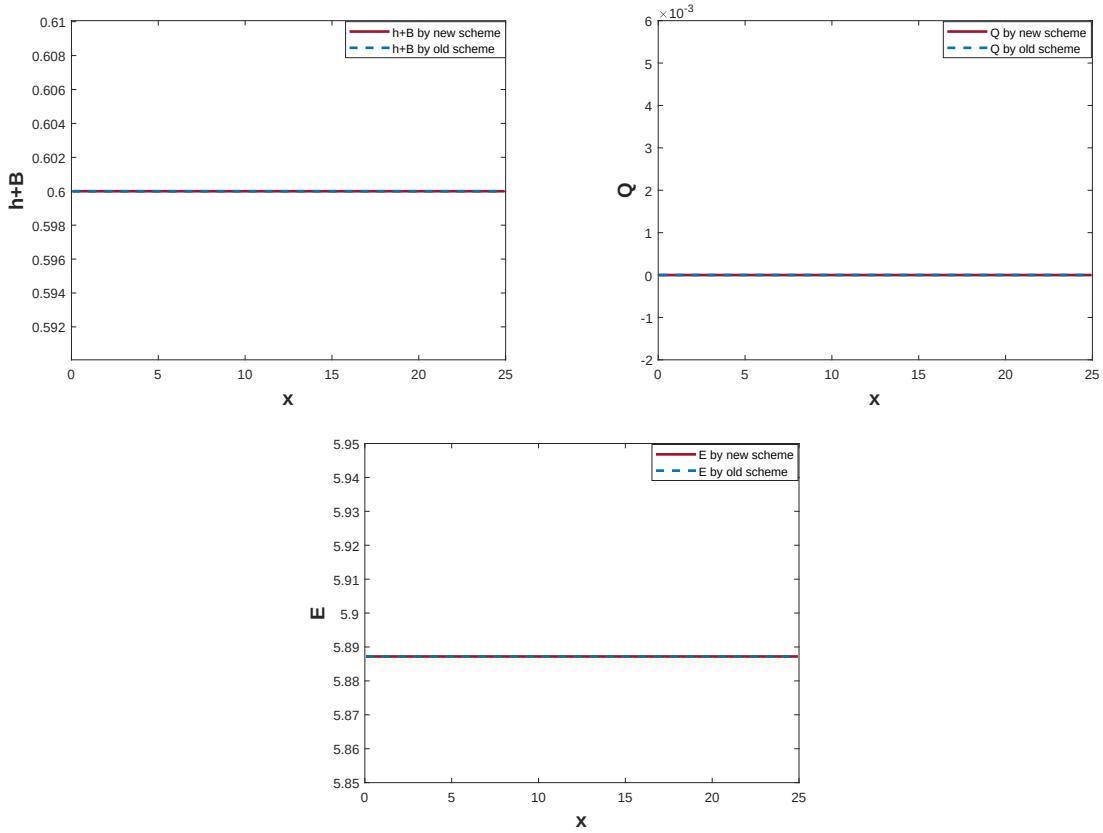

Fig. 4.1 still-water steady states at $t = 20$.

4.3. Steady-state solution of moving-water.

In this experiment we wish to verify whether the scheme proposed in this paper has the well-balanced property of convergence to the moving-water steady states. The channel through which the water flows during the experimental tests is an irregular channel with a bulge at the bottom. The bottom topography and channel width are:

$$B(x) = \begin{cases} 0.2 - 0.05(x-11)^2, & 9 \le x \le 13, \\ 0, & \text{otherwise}, \end{cases} \tag{4.1}$$

Table 4.3 L^1- and L^∞-errors of the discharge Q by the new and old schemes.

	Supercritical flow		Subcritical flow		Transcritical flow	
	New	Old	New	Old	New	Old
L^1-error	4.9752e-10	2.26e-01	9.3233e-11	3.46e-02	1.1088e-11	1.94e-02
L^∞-error	3.8298e-11	9.80e-03	6.9633e-13	8.43e-04	1.1382e-12	2.57e-04

$$\sigma(x) = \begin{cases} 0.8 + 0.05(x-5)^2, & 3 \le x \le 7, \\ 1.18 - 0.02(x-18)^2, & 15 \le x \le 21, \\ 1, & \text{otherwise.} \end{cases} \tag{4.2}$$

Three groups of initial and boundary values are considered below, which correspond to three different steady-state solutions: supercritical, subcritical, and transcritical. We test these conditions, respectively, for numerical experiments, which are taken from the reference [12]:

(a) Initial and boundary conditions of supercritical flow:

$$\begin{aligned} A(x,0) = \sigma(x)\cdot[2 - B(x)], \quad Q(x,0) \equiv 0, \\ A(0,t) = 2\sigma(0), \quad Q(0,t) = 24\sigma(0). \end{aligned} \tag{4.3}$$

(b) Initial and boundary conditions of subcritical flow:

$$\begin{aligned} A(x,0) = \sigma(x)\cdot[2 - B(x)], \quad Q(x,0) \equiv 0, \\ Q(0,t) = 4.42\sigma(0), \quad A(25,t) = 2\sigma(25). \end{aligned} \tag{4.4}$$

(c) Initial and boundary conditions of transcritical flow:

$$\begin{aligned} A(x,0) = \sigma(x)\cdot[0.66 - B(x)], \quad Q(x,0) \equiv 0, \\ Q(0,t) = 1.53\sigma(0), \quad A(25,t) = 0.66\sigma(25). \end{aligned} \tag{4.5}$$

REMARK 4.1. *In the numerical experiment for the transcritical flow, we impose the downstream boundary value* $A(25,t) = 0.66\sigma(25)$ *when the flow is subsonic.*

In these three numerical experiments, we set the experiment to end at $t = 400$. In Figures 4.2-4.4, we show the results: $h + B$, Q and E for the two schemes. It is clear to see that the New scheme exactly captures the moving-water steady-states solutions at these flow, while the Old Scheme fails to converge and generate nonphysical peaks.

At the same time, we compare the errors (L^1-errors and L^∞-errors) in their calculated variables Q with the exact solutions of the Old and New schemes and show the results obtained numerically in Table 4.3. This further illustrates that the New scheme converges and maintains the moving-water steady states, while the Old scheme generates relatively large errors. Therefore, the numerical results and error analysis can clearly show that the scheme proposed in this paper has well-balanced property for convergence to the moving-water steady states.

4.4. Small perturbation propagation in moving-water steady states.

In this experiment we verify whether the scheme proposed in this paper has the ability to accurately capture the propagation of small perturbations in the steady-state solution. If the scheme is not well-balanced, it is not able to capture the perturbations well and accurately. The bottom topography function

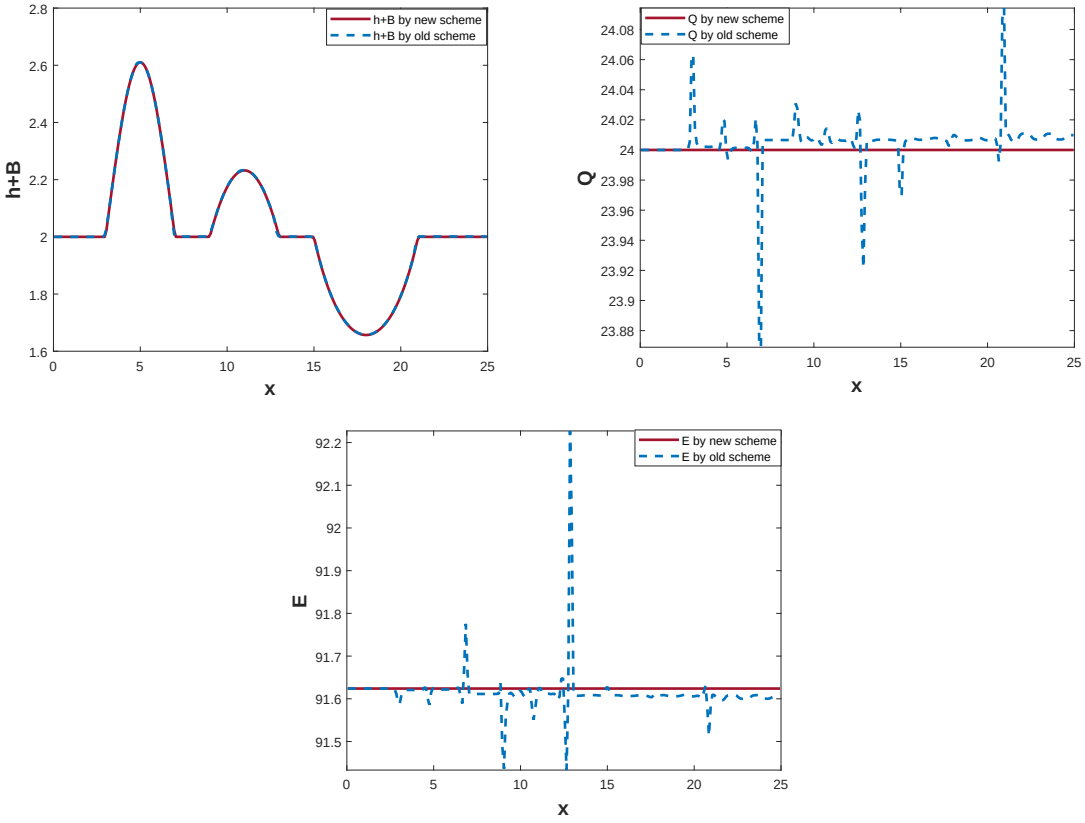

Fig. 4.2 case (a): $h+B$, Q and E for supercritical flows.

and the channel width function are the same as those of Example 4.3, with the following initial conditions, respectively:

(a)Conditions of supersonic flow:

$$Q(x,0) \equiv 24, \quad E(x,0) \equiv \frac{24^2}{2\times 2^2} + 9.812 \times 2. \tag{4.6}$$

(b)Conditions of subsonic flow:

$$Q(x,0) \equiv 4.42, \quad E(x,0) \equiv \frac{4.42^2}{2\times 2^2} + 9.812 \times 2. \tag{4.7}$$

(c)Conditions of transcritical flow:

$$Q(x,0) \equiv 1.53, \quad E(x,0) \equiv \frac{3}{2}(9.812\times 1.53)^{\frac{2}{3}} + 9.812 \times 0.2. \tag{4.8}$$

Based on the final steady states in Example 4.3, we add a small positive number $\epsilon = 0.05\sigma(x)$ to the A in the interval $x \in [5.75, 6.25]$. We use the two schemes to calculate numerical solutions until $t = 1$ in Case (a) while $t = 1.5$ in Cases (b) and (c). The difference between the calculated water depth h and the background moving steady-state water depth are shown in Figures 4.5-4.7. Then, we reduce the small positive number to $\epsilon = 0.001\sigma(x)$ and show the difference in Figures 4.8-4.10. We note that the New scheme produces no spurious oscillations on the raised bottom compared to the Old scheme and captures the propagation perturbations well under different flows.

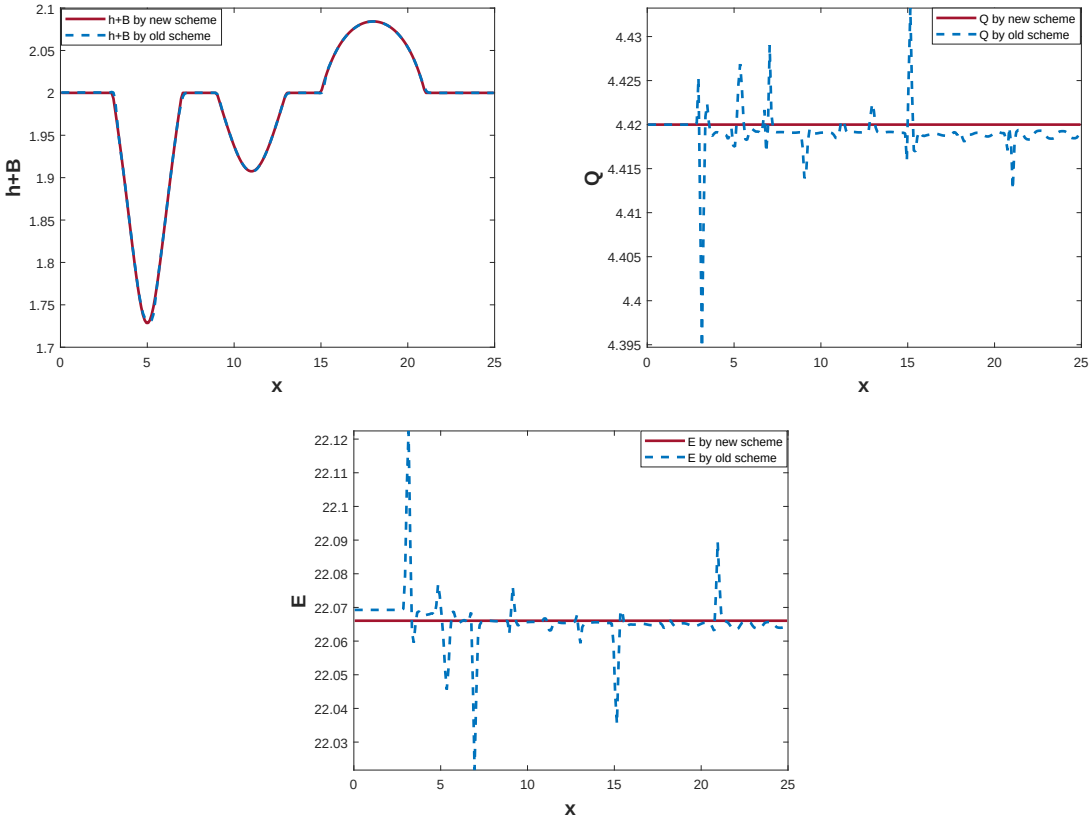

Fig. 4.3 case (b): $h+B$, Q and E for subcritical flows.

4.5. Dam-break experiments.

During this numerical experiment, we numerically simulate the proposed scheme to deal with the dam-break problem in a non-constant width channel with an initial irregular dry bed. The channel width function and bottom topography function are:

$$\sigma(x) = \begin{cases} 0.8 + 0.002(x-13)^2, & 3 \le x \le 23, \\ 1.0, & \text{otherwise}, \end{cases} \qquad B(x) = \begin{cases} 0.2 - 0.05(x-11)^2, & 9 \le x \le 13, \\ 0, & \text{otherwise}. \end{cases}$$

other data are

$$A(x,0) = \begin{cases} 2\sigma(x), & x < 5, \\ 0, & \text{otherwise}, \end{cases} \qquad Q(x,0) = \begin{cases} 24\sigma(x), & x < 5, \\ 0, & \text{otherwise}. \end{cases}$$

We use the same boundary condition as in case (a) of Example 4.3. In Figure 4.11, we show results for $t = 0.1,\ 0.5,\ 1,\ 2,\ 8$. We can see that the New scheme is stable and does not generate non-physical high Q values at the wet and dry interfaces. When $t = 8$ the water flow reaches the steady states. This experiment also verifies the positivity-preserving and robust of the proposed scheme.

5. Conclusion.

In this paper, for open channel flows with variable river width and non-flat bottom, we proposed a non-staggered central scheme with second-order accuracy on both time and space scales. To begin with, a piecewise linear approximation was made for the variable river width and the non-flat bottom in order

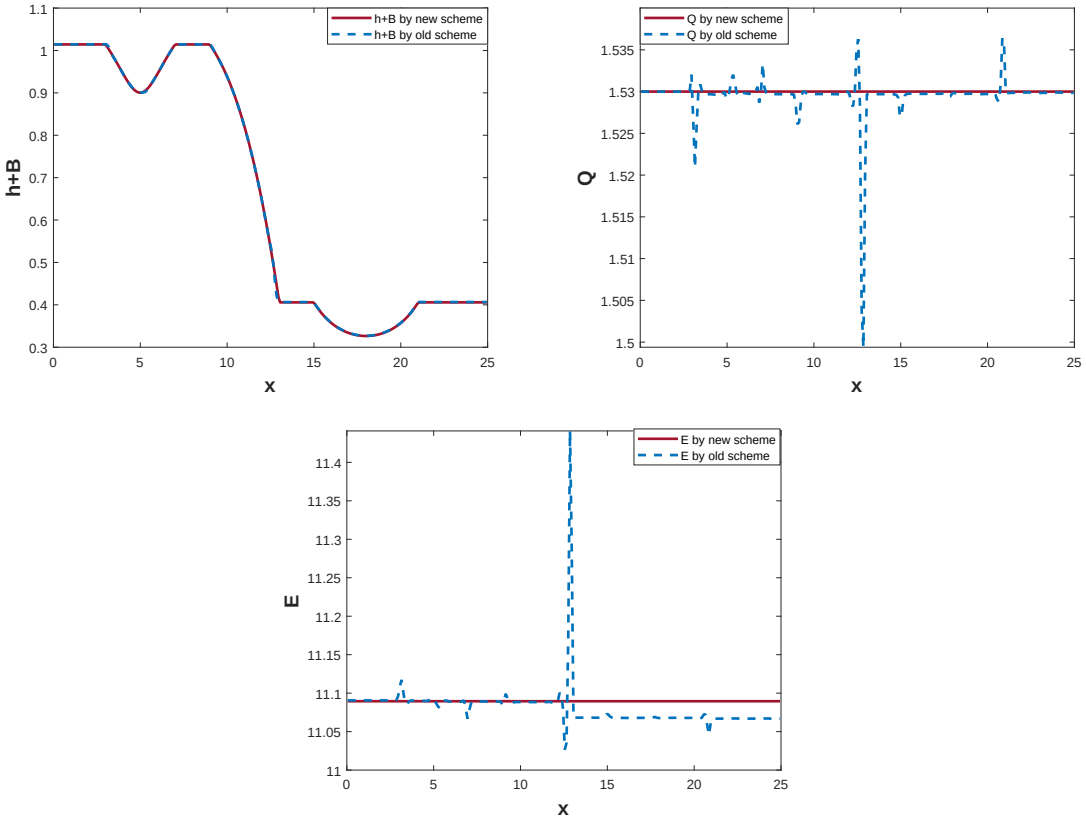

Fig. 4.4 case (c): $h + B$, Q and E for transcritical flows.

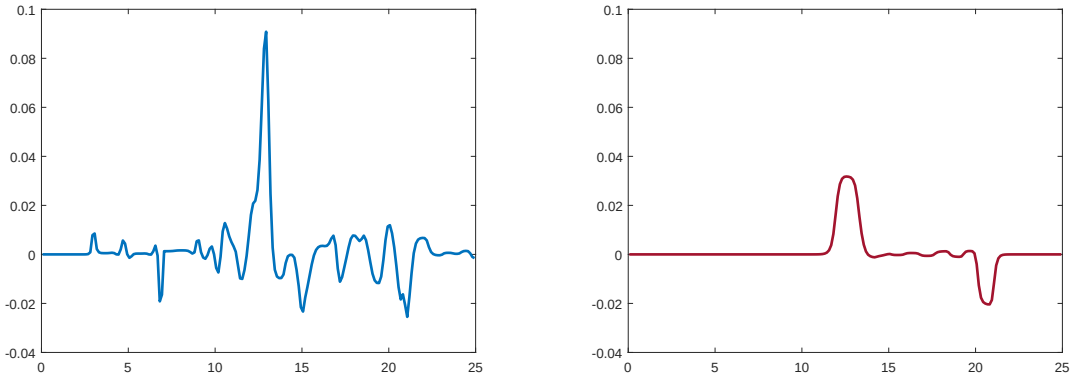

Fig. 4.5 case (a): the difference between obtained h and the background moving steady-state h for the old (left) scheme and the new (right) scheme(cells=200, $\epsilon = 0.05$).

to simplify the calculation. Next, in the forward step, by piecewise linear reconstruction of the conserved variables and energy, the scheme was spatially accurate to the second order and oscillations can be avoided. Moreover, in considering the energy balance, we solved the nonlinear equations by choosing the root that are related to the physical significance. Then, in the correction step, we utilized this property that the energy of the equilibrium variable remains constant to discretize the complex source term thus keeping the source terms and fluxes able to balance exactly. Also, in purpose of maintaining the positivity of the wet cross-sectional area, we introduced a "draining" time step technique. Finally, in the backward step, we

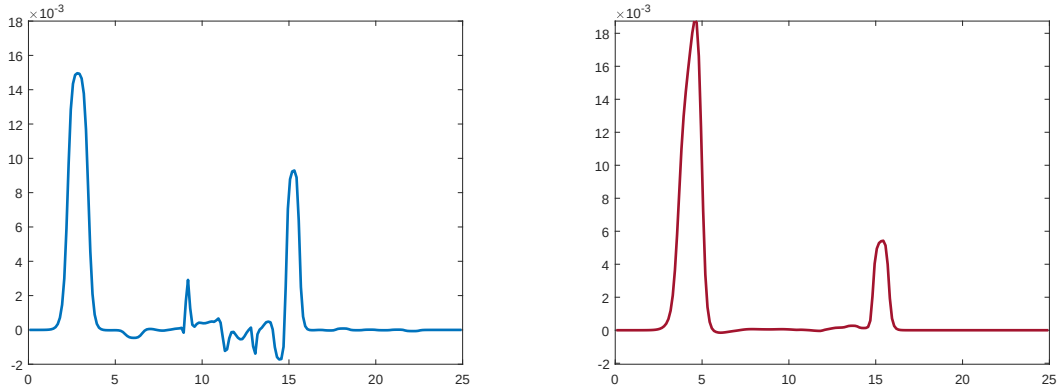

Fig. 4.6 case (b): the difference between obtained h and the background moving steady-state h for the old (left) scheme and the new (right) scheme(cells=200, $\epsilon = 0.05$).

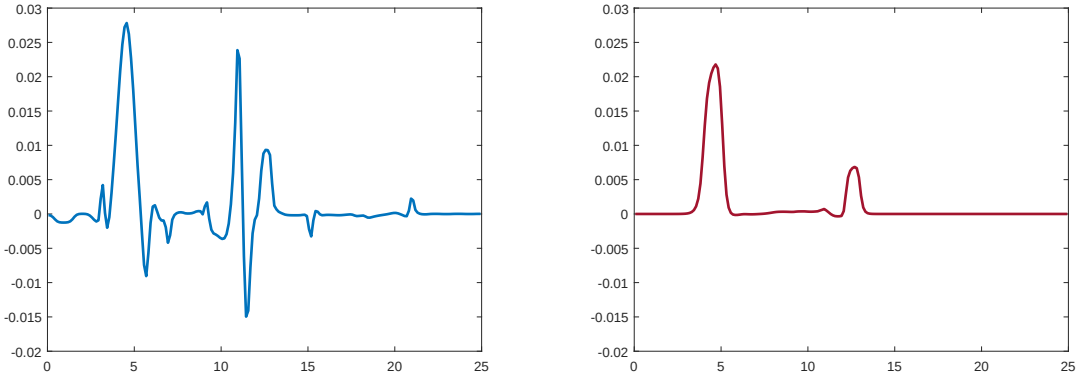

Fig. 4.7 case (c): the difference between obtained h and the background moving steady-state h for the old (left) scheme and the new (right) scheme(cells=200, $\epsilon = 0.05$).

obtained the solutions on the non-staggered grid by the same treatment of cell averaging of the solutions on the staggered grid as in the forward step.

Numerical experiments showed that the scheme can maintain not only the moving-water steady-state solution but also the still-water steady-state solution, as well as accurately capture small perturbations in the moving-water steady-state solution. The dam-break experiments also exemplified that the scheme is positive-preserving and robust.

This work is the first to use a non-staggered central scheme to maintain the moving-water steady-state solution. This scheme does not require the use of a Riemann solver, so it is computationally much simpler. Moreover, the scheme is able to maintain both types of steady-state solutions simultaneously.

6. Acknowledgments.

Thanks to Prof. Lu's guidance, some practical problems of fluid mechanics they faced in engineering are very inspiring for us in the study of the theory. This work was supported in part by the National Natural Science Foundation of China (No.11971481, No.51879194).

REFERENCES

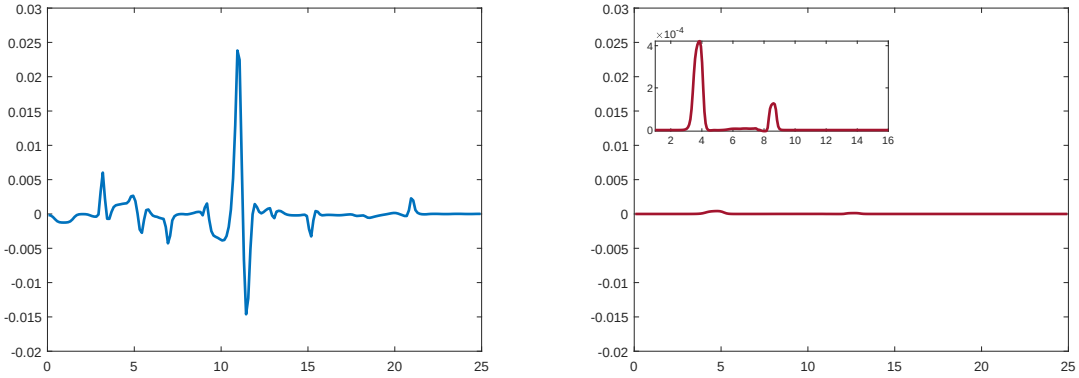

Fig. 4.8 case (a): the difference between obtained h and the background moving steady-state h for the old (left) scheme and the new (right) scheme(cells=200, $\epsilon = 0.001$).

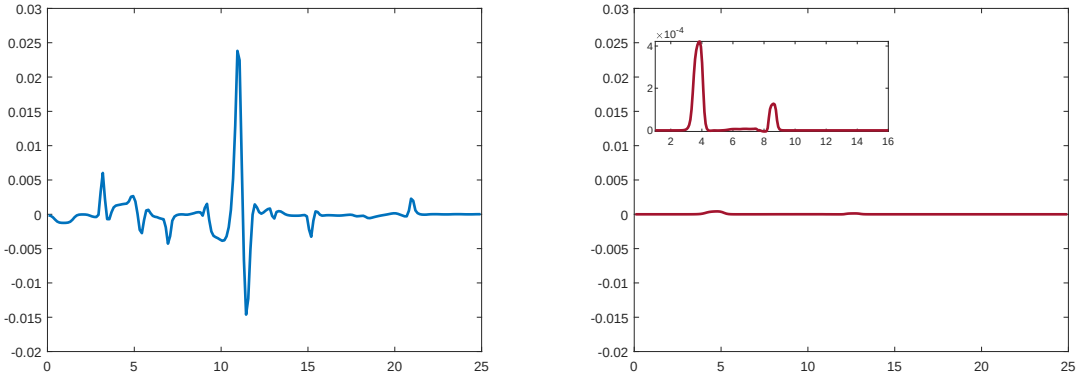

Fig. 4.9 case (b): the difference between obtained h and the background moving steady-state h for the old (left) scheme and the new (right) scheme(cells=200, $\epsilon = 0.001$).

[1] Murillo, J., García-Navarro, P.: *Accurate numerical modeling of 1D flow in channels with arbitrary shape. Application of the energy balanced property.* J. Comput. Phys. 260, 222-248(2014)
[2] Liu, X.: *A steady-state-preserving scheme for shallow water flows in channels.* J. Comput. Phys. 423, 109803(2020)
[3] Liu, X., Chen, X., Jin, S., Kurganov, A., Wu, T., Yu, H.: *Moving-Water Equilibria Preserving Partial Relaxation Scheme for the Saint-Venant System.* SIAM J. Sci. Comput. 42(4), A2206-A2229(2020)
[4] Kurganov, A., Petrova, G.: *A second-order well-balanced positivity preserving central-upwind scheme for the Saint-Venant system.* Commun. Math. Sci. 5, 133-160(2007)
[5] Cheng, Y.Z., Kurganov, A.: *Moving-water equilibria preserving central-upwind schemes for the shallow water equations.* Commun. Math. Sci. 14(6), 1643-1663(2016)
[6] Cheng, Y.Z., Chertock, A., Herty, M., Kurganov, A., Wu, T.: *A New Approach for Designing Moving-Water Equilibria Preserving Schemes for the Shallow Water Equations.* J. Sci. Comput. 80(1), 538-554(2019)
[7] Xing, Y.L., Shu, C.W., Noelle, S.: *On the advantage of well-balanced schemes for moving-water equilibria of the shallow water equations.* J. Sci. Comput. 48(1), 339-349(2011)
[8] Xing, Y.L.: *Exactly well-balanced discontinuous Galerkin methods for the shallow water equations with moving water equilibrium.* J. Comput. Phys. 257, 536-553(2014)
[9] Nessyahu, H., Tadmor, E.: *Non-oscillatory central differencing for hyperbolic conservation laws.* J. Comput. Phys. 87(2), 408-463(1990)
[10] Jiang, G.S., Levy, D., Lin, C.T., Osher, S., Tadmor, E.: *High-resolution nonoscillatory central schemes with nonstaggered grids for hyperbolic conservation laws.* SIAM J. Numer. Anal. 35(6), 2147-2168(1998)
[11] Russo, G., Khe, A. : *High order well balanced schemes for systems of balance laws, in Hyperbolic problems: theory numerics and applications.* Proc. Sympos. Appl. Math., Amer. Math. Soc., Providence, RI 67, 919-928(2009)
[12] Khan, A.A., Lai, W.: *Modeling Shallow Water Flows using the Discontinuous Galerkin Method.* New York: CRC Press (2014)
[13] Liu, X.D., Tadmor, E.: *Third order nonoscillatory central scheme for hyperbolic conservation laws.* Numer. Math. 79(3),

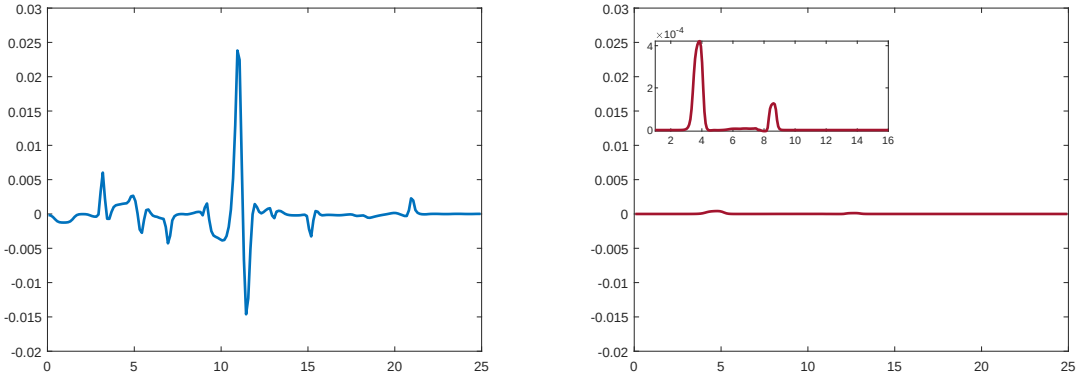

Fig. 4.10 case (c): the difference between obtained h and the background moving steady-state h for the old (left) scheme and the new (right) Scheme(cells=200, $\epsilon = 0.001$).

397C425(1998)

[14] Jiang, G.S., Tadmor, E.: *Nonoscillatory central schemes for multidimensional hyperbolic conservation laws*. SIAM J. Sci. Comput. 19(6), 1892C1917(1998)

[15] Levy, D., Puppo, G., Russo, G.: *Central weno schemes for hyperbolic systems of conservation laws*. ESAIM: Math. Model. Numer. Anal. 33(3), 547C571(1999)

[16] Levy, D., Puppo, G., Russo, G.: *Compact central weno schemes for multidimensional conservation laws*. SIAM J. Sci. Comput. 22(2), 656C672(2000)

[17] Dong, J., Li, D.F.: *An effect non-staggered central scheme based on new hydrostatic reconstruction*. App. Math. Comput. 372, 124992(2020)

[18] Dong, J., Li, D.F.: *Exactly well-balanced positivity preserving nonstaggered central scheme for open-channel flows*. Int. J. Numer. Meth. Fl. 93(1), 273-292(2021)

[19] Dong, J.: *A robust second-order surface reconstruction for shallow water flows with a discontinuous topography and a Manning friction*. Adv. Comput. Math. 46(2), 1-33(2020)

[20] Balbás, J. ,Hernandez-Duenas, G.: *A positivity preserving central scheme for shallow water flows in channels with wet-dry states*. ESAIM: Math. Model. Numer. Anal. 48, 665-696(2014)

[21] Balbás, J.,Karni, S.: *A central scheme for shallow water flows along channels with irregular geometry*. ESAIM: Math. Model. Num. Anal. 43(2), 333-351(2009)

[22] Touma, R., Khankan, S.: *Well-balanced unstaggered central schemes for one and two-dimensional shallow water equation systems*. Appl. Math. Comput. 218(10), 5948-5960(2012)

[23] Touma, R.: *Well-balanced central schemes for systems of shallow water equations with wet and dry states*. Appl. Math. Model 40(4), 2929C2945(2016)

[24] Qian, S.G., Li, G., Shao, F., Xing, Y.: *Positivity-preserving well-balanced discontinuous galerkin methods for the shallow water flows in open channels*. Adv. Water Resour. 115 ,172-184(2018)

[25] Vázquez-Cendón, ME.: *Improved Treatment of Source Terms in Upwind Schemes for the Shallow Water Equations in Channels with Irregular Geometry*. J. Comput. Phys. 148(2), 497-526(1999)

[26] Hernández-Dueñas, G. : *Shallow water flows in channels*. J. Sci. Comput. 48(1-3), 190-208(2011)

[27] Shu, C.W.: *Total-variation-diminishing time discretizations*. SIAM J. Sci. Comput. 6, 1073-1084(1988)

[28] Noelle, S., Xing, Y., Shu, C.W.: *High-order well-balanced finite volume WENO schemes for shallow water equation with moving water*. J. Comput. Phys. 226, 29C58(2007)

[29] Bollermann, A., Noelle, S., Lukáčová-Medviďová, M.: *Finite volume evolution Galerkin methods for the shallow water equations with dry beds*. Commun. Comput. Phys. 10, 371-404(2011)

[30] Xing, Y.L.: *High-order finite volume WENO schemes for the shallow water flows through channels with irregular geometry*. J. Comput. Appl. Math. 299, 229-244(2016)

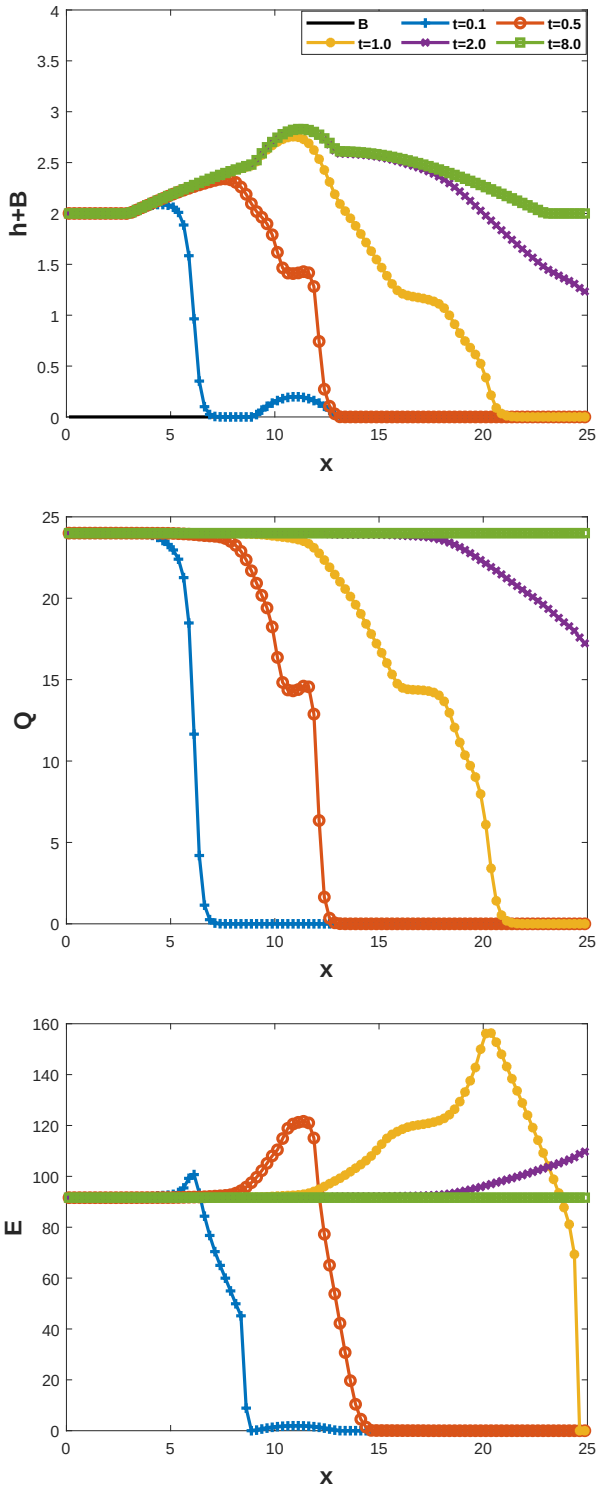

Fig. 4.11 Dam break: Computed $h + B$ (top), Q (middle) and E (bottom).